

# Validity test of the “Trojan horse” method applied to the ${}^6\text{Li}(p,\alpha){}^3\text{He}$ reaction

A. Tumino,<sup>1,2</sup> C. Spitaleri,<sup>1,2</sup> A. Di Pietro,<sup>2</sup> P. Figuera,<sup>2</sup> M. Lattuada,<sup>2,3</sup> A. Musumarra,<sup>1,2</sup> M. G. Pellegriti,<sup>1,2</sup> R. G. Pizzone,<sup>1,2</sup> S. Romano,<sup>1,2</sup> C. Rolfs,<sup>4</sup> S. Tudisco,<sup>1,2</sup> and S. Typel<sup>5</sup>

<sup>1</sup>Dipartimento di Metodologie Fisiche e Chimiche per l’Ingegneria, Università di Catania, Catania, Italy

<sup>2</sup>Laboratori Nazionali del Sud-INFN, Catania, Italy

<sup>3</sup>Dipartimento di Fisica e Astronomia, Università di Catania, Catania, Italy

<sup>4</sup>Ruhr-Universität, Bochum, Germany

<sup>5</sup>Gesellschaft für Schwerionenforschung mbH, Theorie, Darmstadt, Germany

(Received 19 November 2002; published 20 June 2003)

The  ${}^6\text{Li}(p,\alpha){}^3\text{He}$  reaction has been studied from  $E_{\text{c.m.}} = 2.4$  MeV down to astrophysical energies by means of the indirect Trojan horse method applied to the  ${}^2\text{H}({}^6\text{Li},\alpha{}^3\text{He})n$  three-body reaction performed at an incident energy of 25 MeV. Coincidence spectra measured in a kinematically complete experiment show the presence of the quasifree  ${}^6\text{Li}-p$  process. The excitation function for this process was extracted from the three-body reaction cross section at low neutron momentum and compared with the behavior of the free two-body reaction cross section.

DOI: 10.1103/PhysRevC.67.065803

PACS number(s): 26.20.+f, 21.10.Pc, 24.50.+g, 25.70.Hi

## I. INTRODUCTION

Among indirect methods to study charged particle reactions at astrophysical energies, e.g., Coulomb dissociation [1,2] and the asymptotic normalization coefficient method [3–6], the Trojan horse method (THM) [7–9] has proven to be a very powerful tool since it makes it possible to compensate the exponential decrease of the cross section at sub-Coulomb energies. Once selected, the quasifree contribution of an appropriate three-body reaction performed at energies well above the Coulomb barrier, the off-shell cross section of the astrophysically relevant two-body reaction can be extracted even at very low relative energy. A number of reactions, such as  ${}^7\text{Li}(p,\alpha){}^4\text{He}$  and  ${}^6\text{Li}(d,\alpha){}^4\text{He}$ , connected with fundamental astrophysical problems [10,11] have already been studied through the  $d({}^7\text{Li},\alpha\alpha)n$  [12–16] and the  ${}^6\text{Li}({}^6\text{Li},\alpha\alpha){}^4\text{He}$  [17,18] three-body reactions, respectively. Important results were obtained and those studies allowed to validate the conditions under which the method can be applied at energies above and below the Coulomb barrier, although not within the same experiment. The present paper reports on a recent investigation of the  ${}^6\text{Li}(p,\alpha){}^3\text{He}$  reaction through the  ${}^2\text{H}({}^6\text{Li},\alpha n){}^3\text{He}$  three-body reaction. A wide range of  $E_{\text{c.m.}}$  for the  ${}^6\text{Li}-p$  system was explored, allowing to perform a complete validity test of the THM below and above the Coulomb barrier at the same time. Besides a non-resonant  $s$ -wave contribution, the  ${}^6\text{Li}(p,\alpha){}^3\text{He}$  two-body reaction appears to proceed through a state of the intermediate  ${}^7\text{Be}$  nucleus at 7.2-MeV excitation energy, which produces a resonance at  $E_{\text{c.m.}} = 1.6$  MeV in the  ${}^6\text{Li}-p$  excitation function [19–22]. A noticeable result would mean the presence of the same resonant behavior in the  ${}^6\text{Li}-p$  excitation function indirectly extracted. The quasifree contribution to the  ${}^2\text{H}({}^6\text{Li},\alpha n){}^3\text{He}$  reaction was previously investigated at energies above the Coulomb barrier [23]. In spite of the large energy step exploited in that experiment, a fair global agreement with the free reaction cross section was obtained and quasifree data were reproduced quite well by a simple calculation based on the plane-wave impulse approximation [24].

We will employ two steps in the evaluation of the experimental data: first the quasifree contribution to the three-body breakup reaction is selected from the experimental data and compared with the result of a Monte Carlo simulation performed under the assumption of a pure quasifree mechanism; then the two-body excitation function is extracted from the data and compared with the one obtained from a direct  ${}^6\text{Li}(p,\alpha){}^3\text{He}$  experiment. A number of direct datasets concerning the  ${}^6\text{Li}(p,\alpha){}^3\text{He}$  reaction are available, and most of them are accounted for in the NACRE compilation [19–22,26–32]. Here we refer to the data of Ref. [22], which cover the whole energy range investigated in the present work, and whose resonant behavior appears to be well reproduced by the fitted  $S$  factor curve in the NACRE compilation [32].

## II. A REVIEW OF THE THM THEORETICAL FORMALISM

We give a short description of the basic hypotheses of the THM, since it has already been presented several times [8,9,14–16,18]. The THM applies to a reaction between a particle  $A$  and a nucleus  $a$  (the Trojan horse), whose associated wave function has a large amplitude for a  $x-b$  cluster configuration. Under appropriate kinematical conditions it is possible to select the quasifree contribution to the three-body breakup reaction where the particle  $A$  interacts only with the part  $x$  of the nucleus  $a$ , leaving the nucleus  $b$  as a spectator to the process  $A+a(=x+b)\rightarrow C+c+b$ . The  $A+a$  reaction occurs at a center-of-mass (c.m.) energy  $E_{Aa}$  above the Coulomb barrier, chosen in such a way that the quasifree  $A+x$  process can take place even at very low sub-Coulomb energies  $E_{Ax}$ . In this framework, the  $x-b$  binding energy plays a key role in compensating for the  $A+a$  relative motion, determining the so called “quasifree two-body energy” given by

$$E_{\text{qf}} = E_{Ax} - B_{x-b}, \quad (1)$$

equivalent to the expression given in Ref. [9].  $E_{Ax}$  represents the beam energy in the center-of-mass of the two-body  $A$

$-x$  system and  $B_{x-b}$  is the binding energy for the  $x-b$  system. Then, a cutoff in the momentum distribution, which is related to the Fermi motion of  $b$  inside the Trojan horse  $a$ , fixes the range of energies  $E_{Ax}$  around the “quasifree two-body energy” accessible in the astrophysically relevant reaction. Since the Trojan horse method effectively removes the Coulomb barrier for the system  $A-x$ , their collision takes place in the nuclear interaction region without suffering from either Coulomb suppression or electron screening effects. A detailed theoretical formalism has been employed in a post-form distorted-wave Born description to derive the relation between the triple differential cross section of the three-body breakup reaction and the two-body cross section of interest [8,9]. In this approach the surface approximation is employed in order to derive an expression of the three-body  $T$ -matrix element in terms of the  $S$ -matrix elements of the astrophysical two-body reaction. A further and simpler description in terms of a modified plane-wave approximation leads to a form for the three-body cross section similar to that of the plane-wave impulse approximation [24]. The modified plane-wave approximation still accounts for the Coulomb effects in the two-body reaction, but neglects them in the entrance and exit channels of the three-body reaction. As long as the energies involved are high enough, as in the present case, this does not change the energy dependence of the astrophysical relevant two-body cross section but only its absolute magnitude. Therefore, the THM can be used to extract the energy dependence of the two-body reaction. However, the absolute magnitude of the cross section has to be derived from a scaling to direct data available at higher energies.

Here we give only the most relevant formulas. For details we refer to Refs. [8,9]. Using the above approximations, the triple differential cross section is given by

$$\frac{d^3\sigma}{dE_C d\Omega_C d\Omega_c} = KF |W(\vec{Q}_{Bb})|^2 \frac{16\pi^2}{k_{Ax}^2 Q_{Aa}^2} \frac{v_{Cc}}{v_{Ax}} \frac{d\sigma^{TH}}{d\Omega} \quad (2)$$

with momenta

$$\hbar \vec{Q}_{Aa} = \vec{p}_{Aa} - \frac{m_A}{m_A + m_x} \vec{p}_{Bb}, \quad \hbar \vec{Q}_{Bb} = \vec{p}_{Bb} - \frac{m_b}{m_b + m_x} \vec{p}_{Aa}, \quad (3)$$

and a momentum amplitude  $W(\vec{Q}_{Bb})$  that is connected to the wave function of the Trojan horse  $a$  in momentum space. For the present case the deuteron is the Trojan horse where we assume a Hulthén wave function

$$\Phi(\vec{r}) = \sqrt{\frac{ab(a+b)}{2\pi(a-b)^2}} \frac{1}{r} (e^{-ar} - e^{-br}) \quad (4)$$

with parameters  $a=0.2317 \text{ fm}^{-1}$  and  $b=1.202 \text{ fm}^{-1}$  [12] for its ground state. KF is a kinematical factor, given by

$$KF = \frac{\mu_{Aa} m_c}{(2\pi)^5 \hbar^7} \frac{p_C p_c^3}{p_{Aa}} \left[ \left( \frac{\vec{p}_{Bb}}{\mu_{Bb}} - \frac{\vec{p}_{Cc}}{m_c} \right) \cdot \frac{\vec{p}_c}{p_c} \right]^{-1} \quad (5)$$

in obvious notation for (relative) momenta and (reduced) masses, where  $B$  denotes the  $C+c$  system. The two-body THM cross section in Eq. (2) is given by

$$\frac{d\sigma^{TH}}{d\Omega} = \frac{1}{4k_{Cc}^2} \left| \sum_l (2l+1) P_l(\hat{Q}_{Aa} \cdot \hat{k}_{Cc}) [S_l J_l^{(+)} - \delta_{(Ax)(Cc)} J_l^{(-)}] \right|^2 \quad (6)$$

with the total (nuclear + Coulomb)  $S$ -matrix elements  $S_l$  for the reaction  $C+c \rightarrow A+x$ , where  $\delta_{(Ax)(Cc)}$  is the Kronecker symbol. It has the form of a usual two-body cross section except for the functions

$$J_l^{(\pm)} = k_{Ax} Q_{Aa} \int_R^\infty dr r j_l(Q_{Aa} r) u_l^{(\pm)}(k_{Ax} r), \quad (7)$$

which reflect the off-shell nature of the two-body process. These functions are given in terms of spherical Bessel functions  $j_l$  and Coulomb wave functions  $u_l^{(\pm)} = e^{\mp i\sigma_l} (G_l \pm iF_l)$ . The integral is calculated starting from the so called cutoff radius  $R$ , which is introduced in the surface approximation and is usually chosen as the sum of the radii of nuclei  $A$  and  $x$ . The argument of the Legendre polynomial  $P_l$  in Eq. (3) corresponds to the cosine of the c.m. scattering angle of the two-body reaction. For small energies  $E_{Ax} = \hbar^2 k_{Ax}^2 / (2\mu_{Ax})$  in the  $A+x$  channel, i.e., small  $k_{Ax}$  and a large Sommerfeld parameter  $\eta_{Ax}$ , the main contribution to the integral derives from radii close to the cutoff radius  $R$ , due to the behavior of the irregular Coulomb function  $G_l$  in  $u_l^{(\pm)}$  that increases rapidly for small radii. Thus, we use

$$J_l^{(\pm)} \approx k_{Ax} Q_{Aa} R^2 j_l(Q_{Aa} R) u_l^{(\pm)}(k_{Ax} R) \quad (8)$$

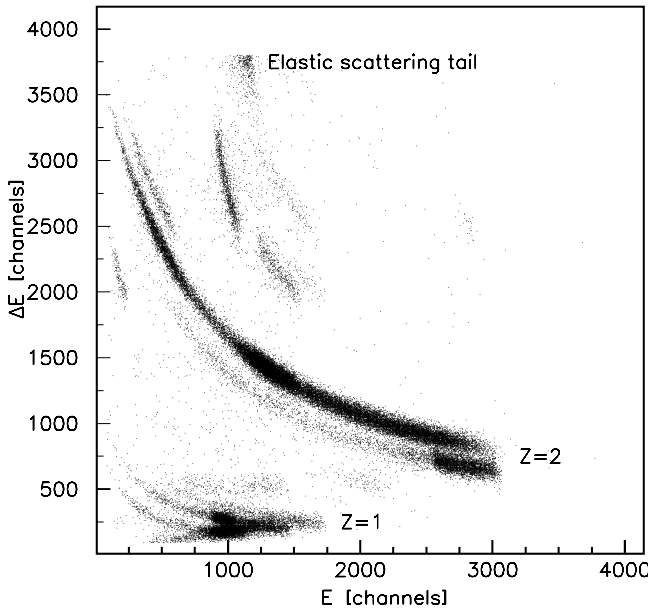
as a first approximation to the integral which contains the essential dependence on the energy  $E_{Ax}$ . Since the quantity  $Q_{Aa}$  is almost constant for small  $Q_{Bb}$  (i.e., in the peak of the momentum distribution) the dependence of the functions  $J_l^{(\pm)}$  on the energy  $E_{Ax}$  is given by  $k_{Ax} u_l^{(\pm)}(k_{Ax} R)$ . For inelastic processes involving different initial and final channels the  $J_l^{(-)}$  term in Eq. (3) vanishes. Thus, Eq. (2) reduces to the more simplified form

$$\frac{d^3\sigma}{dE_C d\Omega_C d\Omega_c} = KF |W(\vec{Q}_{Bb})|^2 \frac{v_{Cc}}{v_{Ax}} \sum_l P_l C_l \frac{d\sigma_l}{d\Omega} (Cc \rightarrow Ax), \quad (9)$$

where we neglected the interference from different partial waves  $l$ . The quantity  $d\sigma_l/d\Omega$  represents the on-shell two-body cross section for the reaction  $C+c \rightarrow A+x$  in partial wave  $l$ , whose Coulomb suppression at low energies is compensated for by the presence of the penetrability factor

$$P_l(k_{Ax} R) = G_l^2(k_{Ax} R) + F_l^2(k_{Ax} R), \quad (10)$$

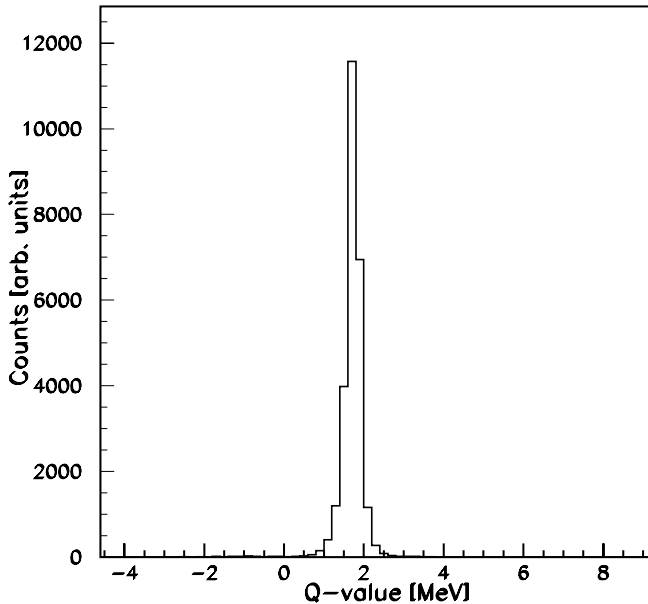
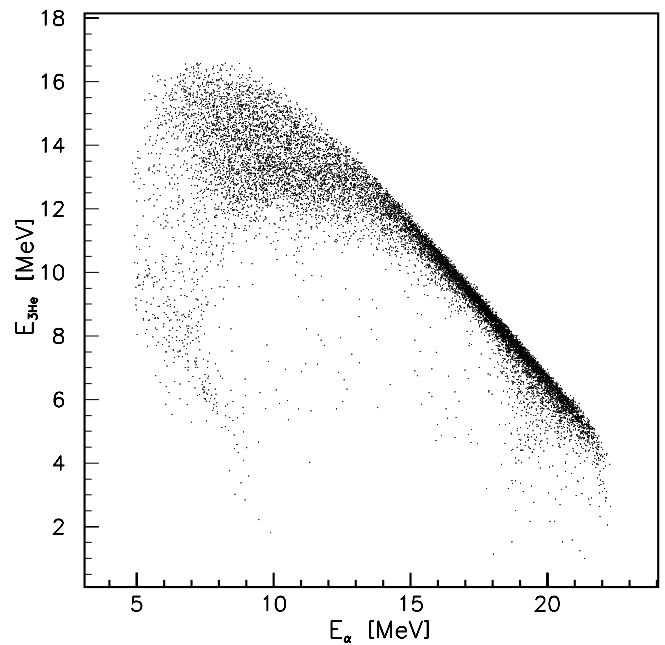
and  $C_l$  is a constant. Expression (10) strongly resembles the factorization resulting from a plane-wave impulse approximation [24] further corrected for the Coulomb penetration.

FIG. 1. Example of a  $\Delta E$ - $E$  matrix for telescope  $T1$ .

The *a priori* inclusion of Coulomb and off-shell effects is indeed the essential feature of the present approach. The appearance of the constant factor  $C_1$  and the employed approximations prevent the absolute value of the two-body cross section to be known. Nevertheless, absolute cross sections can be obtained through normalization to direct data available for most reactions of astrophysical interest at energies above the Coulomb barrier.

### III. THE EXPERIMENT

The experimental study of the  $^2\text{H}(^6\text{Li}, \alpha^3\text{He})n$  reaction was performed with the SMP Tandem van de Graaff accel-

FIG. 2. Experimental  $Q$ -value spectrum for the  $^3\text{He} + \alpha + n$  channel.FIG. 3. Kinematic locus of events  $E_{^3\text{He}}$  vs  $E_\alpha$  within the peak in the  $Q$ -value spectrum of Fig. 2.

erator at the Laboratori Nazionali del Sud in Catania. A  $200 \mu\text{g}/\text{cm}^2$   $\text{CD}_2$  target was bombarded with a 25-MeV  $^6\text{Li}$  beam, with a spot size on target of about 1-mm diameter. The experimental setup consisted of two  $\Delta E - E$  telescopes with  $20\text{-}\mu\text{m}$  silicon detectors as  $\Delta E$  and  $1000\text{-}\mu\text{m}$  position sensitive detectors (PSD) as  $E$  detector. The two telescopes, called  $T1$  and  $T2$  in the following, were placed on opposite sides of the beam direction covering the laboratory angles  $14.5^\circ$  to  $24^\circ$  and  $28.3^\circ$  to  $37.7^\circ$ , respectively, with equal solid angles of  $12.5 \text{ msr}$ . These angles were selected in order to fulfil the quasifree condition  $p_{\bar{n}} = 0 \text{ MeV}/c$  for the breakup process of interest when  $\alpha$  and  $^3\text{He}$  were detected and identified in  $T1$  and  $T2$ , respectively. The wide angular ranges allowed to have several quasifree  $(\theta_\alpha, \theta_{^3\text{He}})$  angular pairs contributing to the process and momentum values for the undetected neutron spectator ranging from about  $-100 \text{ MeV}/c$  to about  $100 \text{ MeV}/c$ . The trigger for the event acquisition was given by the coincidence between the hits of the two telescopes. Energy and position signals for the detected particles were processed by standard electronics together with the delay between the time signals for each coincidence event, and sent to the acquisition system for the online monitoring of the experiment.

### IV. DATA ANALYSIS AND RESULTS

The energy and position calibration of the  $\Delta E$  detectors and PSDs was performed using data acquired in preliminary runs of the  $^{12}\text{C}(^6\text{Li}, \alpha)^{14}\text{N}$  reaction at several beam energies, after the identification of the many  $\alpha$  peaks corresponding to well known excited states of  $^{14}\text{N}$ . A standard three-peak  $\alpha$  source was also used. Energy and position resolution were found to be better than 1%. In order to fully identify the channel of interest and to focus on the kinematical conditions

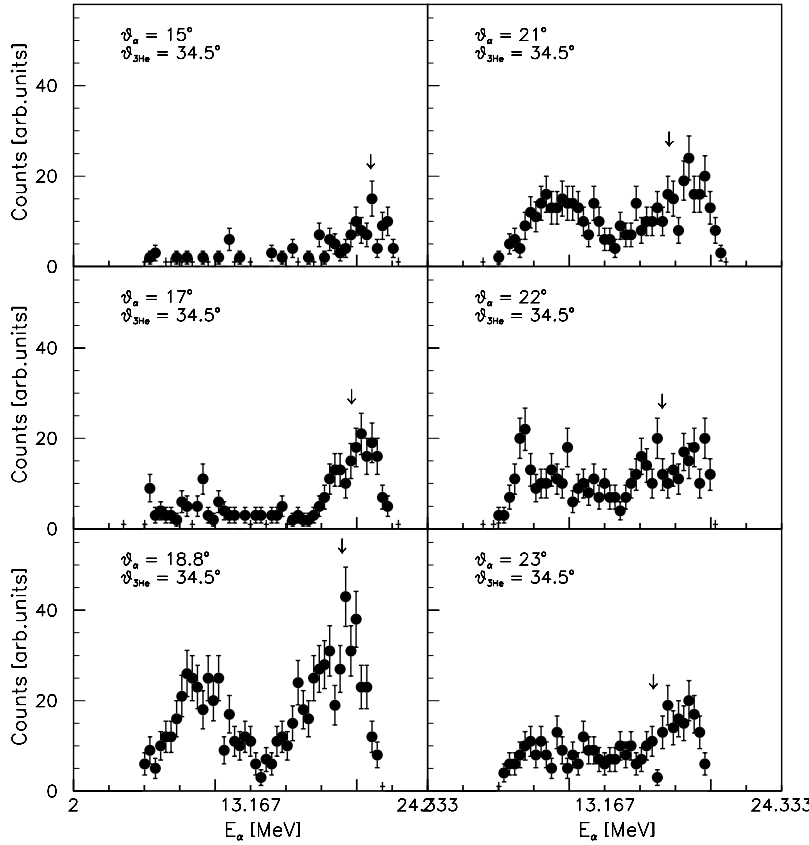


FIG. 4. Coincidence spectra projected on the  $E_\alpha$  axis for a fixed  $\theta_{^3\text{He}}$  and different  $\theta_\alpha$  within angular ranges of  $\pm 0.5^\circ$ . The arrow on the  $E_\alpha$  axis marks the condition corresponding to  $p_n = 0$ .

where the quasifree process should be dominant,  $\alpha$  and  ${}^3\text{He}$  loci have been selected in the  $\Delta E$ - $E$  matrices of the  $T1$  and  $T2$  telescopes, respectively. As an example, the  $\Delta E$ - $E$  matrix for  $T1$  is shown in Fig. 1. Beside the events falling into the  $Z=1$  and  $Z=2$  loci and into the elastic scattering tail (see the figure), the simultaneous detection of two light particles produces the groups of spurious signals in between. These events do not interfere at all in the selection of the  $\alpha$  and  ${}^3\text{He}$  loci for the further analysis, being well separated from them. The kinematics were reconstructed under the assumption of a neutron as third particle, leading to the  $Q$ -value spectrum shown in Fig. 2. The spectrum shows a sharp peak just below 2 MeV, which corresponds to the channel of interest, i.e.,  ${}^3\text{He} + \alpha + n$ , whose calculated  $Q$  value is 1.79 MeV. The corresponding locus of the events in the  $E_{^3\text{He}}$  versus  $E_\alpha$  plane is shown in Fig. 3. The resulting spectra make us confident regarding the quality of the performed calibration, and the possibility to well identify the  ${}^3\text{He} + \alpha + n$  channel. In order to check the presence of the quasifree contribution, coincidence spectra have been projected on the  $E_{^3\text{He}}(E_\alpha)$  axis for a fixed angle of one of the two particles,  $\theta_{^3\text{He}}(\theta_\alpha)$  and varying the other angle within the angular range of the detector. An example of the resulting spectra is shown in Fig. 4. The arrows mark the condition of nearly zero neutron momentum. The feature expected for a quasifree process shows up, that is, the coincidence yield decreases as  $p_n$  moves away from zero, which corresponds to the  $(\theta_{^3\text{He}}, \theta_\alpha) = (34.5^\circ, 18.8^\circ)$  angle pair. Similar results have been obtained for other quasifree angle pairs. Sequential processes through the ground state of  ${}^5\text{He}$  or excited

states of  ${}^7\text{Be}$  or  ${}^4\text{He}$  are expected to feed the  ${}^3\text{He} + \alpha + n$  channel. While the decay from the  ${}^5\text{He}$  ground state leaves the final neutron with a momentum larger than 100 MeV/c, the other two through  ${}^7\text{Be}^*$  and  ${}^4\text{He}^*$  might produce some effect within the quasifree region of the events. In order to check the presence of those contributions, the experimental quasifree momentum distribution for the neutron can be compared with the expected theoretical behavior given in terms of the Hulthén wave function in momentum space [16].

Dividing the quasifree coincidence yield by the kinematic factor, we are left with a quantity that is proportional to the product of the momentum distribution for the neutron with the differential  ${}^6\text{Li}-p$  two-body cross section [see Eq. (11)]. In the region of the selected quasifree angles, energy and angle in the center-of-mass system for the  ${}^6\text{Li}-p$  two-body channel vary within such a restricted range that the differential two-body cross section in this range can be considered almost constant. Then the quantity defined above represents essentially the momentum distribution for the neutron that has to be compared with the Hulthén wave function in momentum space.

From the comparison reported in Fig. 5 a fair agreement shows up in the region approaching zero neutron momentum. In order to single out the region where the quasifree mechanism is dominant, only coincidence events for neutron momenta ranging from  $-30$  MeV/c and  $30$  MeV/c were considered in the further analysis.

The experiment was simulated by means of a Monte Carlo calculation based on the theoretical approach previ-

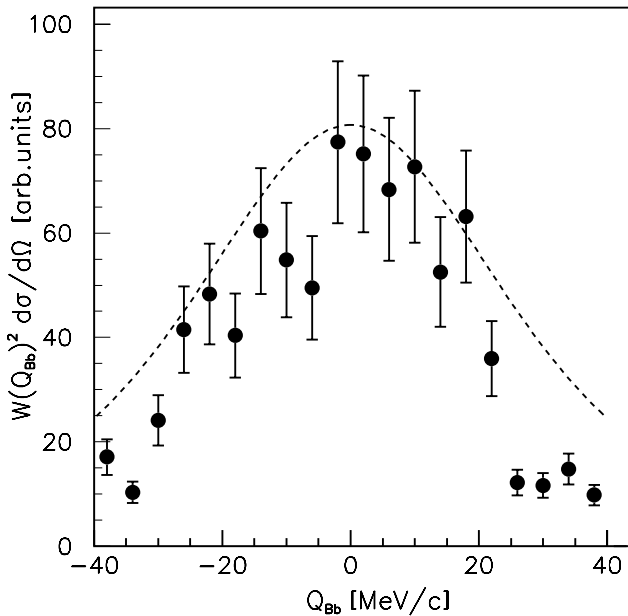


FIG. 5. Experimental momentum distribution for the spectator neutron (full circles), compared with distribution derived from the Hulthén wave function (dashed lines).

ously described. The reaction was assumed to proceed through a pure quasifree mechanism and all experimental constraints in energy and scattering angles for the detected particles were taken into account. The momentum distribution of the neutron inside the deuteron was described in terms of the parametrization given in Ref. [16]. The two-body cross section entering the calculation is the result of a single-level *R*-matrix parametrization of the  ${}^6\text{Li} + p$  reaction [22], taking into account *s* and *p* waves in the entrance channel. The *s*-wave contribution describes the low-energy nonresonant part of the cross section and the *p* wave is responsible of the resonant contribution since the  ${}^6\text{Li} + p$  two-body reaction also proceeds through the  $5/2^-$  resonant state of  ${}^7\text{Be}$  at 7.2 MeV [22]. The level parameter values for the *R*-matrix fit are given in Table I. For all states involved in the *R*-matrix calculation, except for the resonance, a background resonance at 30 MeV was assumed. A channel radius of 4.0 fm was used. The  ${}^2F_{5/2}$  channel in the  ${}^3\text{He} + {}^4\text{He}$  final partition is necessary to describe the resonant structure in the initial *p* wave, as well as to account, together with the  ${}^2D_{3/2}$ , for contributions and couplings in the  $B_L$  coefficients of the angular distributions [22]. The inclusion of the  ${}^2D_{5/2}$  and  ${}^2F_{7/2}$  in the final partition, and of the *d* waves in the initial partition might be needed for a more precise calculation, but, as discussed in Ref. [33], the properties of such levels are too uncertain to make reliable a complete *R*-matrix fit. The result of the *R*-matrix calculation is shown in Fig. 6. Dashed and dotted lines represent the  $l=0$  and  $l=1$  contributions to the two-body cross section, respectively. Their incoherent sum (full line) is superimposed to the direct data from Ref. [22]. Our *R*-matrix fit gives a total  $\chi^2=5.35$  for the cross section, which is rather good for 30 data points and 13 variable parameters. The fit appears to be better than that of Ref. [22], being able to reproduce quite well the behavior of the data in

TABLE I. Level parameters of the *R*-matrix fit:  $J^\pi$ , total angular momentum;  $E_\lambda$ , level energy; *s*, channel spin; *l*, orbital angular momentum; and  $\gamma_{\lambda c}$ , reduced width amplitude.

$J^\pi$	$E_\lambda$ (MeV)	Channel	<i>s</i>	<i>l</i>	$\gamma_{\lambda c}$ (MeV $^{1/2}$ )
$\frac{1}{2}^+$	30.00	${}^6\text{Li} + p$	$\frac{1}{2}$	0	5.3975
$\frac{1}{2}^+$	30.00	${}^3\text{He} + {}^4\text{He}$	$\frac{1}{2}$	0	8.6297
$\frac{3}{2}^+$	30.00	${}^6\text{Li} + p$	$\frac{3}{2}$	0	139.8268
$\frac{3}{2}^+$	30.00	${}^3\text{He} + {}^4\text{He}$	$\frac{1}{2}$	2	4.0860
$\frac{5}{2}^-$	7.15	${}^6\text{Li} + p$	$\frac{3}{2}$	1	0.9375
$\frac{5}{2}^-$	7.15	${}^3\text{He} + {}^4\text{He}$	$\frac{1}{2}$	3	0.1620
$\frac{3}{2}^-$	30.00	${}^6\text{Li} + p$	$\frac{3}{2}$	1	4.6704
$\frac{3}{2}^-$	30.00	${}^6\text{Li} + p$	$\frac{1}{2}$	1	-7.2431
$\frac{3}{2}^-$	30.00	${}^3\text{He} + {}^4\text{He}$	$\frac{1}{2}$	1	2.0540
$\frac{1}{2}^-$	30.00	${}^6\text{Li} + p$	$\frac{3}{2}$	1	1.17516
$\frac{1}{2}^-$	30.00	${}^6\text{Li} + p$	$\frac{1}{2}$	1	1.1043
$\frac{1}{2}^-$	30.00	${}^3\text{He} + {}^4\text{He}$	$\frac{1}{2}$	1	3.7961

the full range. The bump at 0.7 MeV may also partially originate from the contribution of the very broad ( $\Gamma=1.2$  MeV) first  $5/2^-$  level of  ${}^7\text{Be}$  at 6.73 MeV of excitation energy. However, due to its rather large width, this level should not give a substantial improvement to the fit, which in this case would require a more complex two-level *R*-matrix calculation.

The selected coincidence yield, still not corrected for the geometric efficiency of the experimental setup, is shown in Fig. 7 as a function of the  $p$ - ${}^6\text{Li}$  relative energy. A wide  $p$ - ${}^6\text{Li}$  relative energy range is populated, from about 2.5 MeV down to 40 keV. The three-body cross section from the Monte Carlo calculation is also shown (full line), together

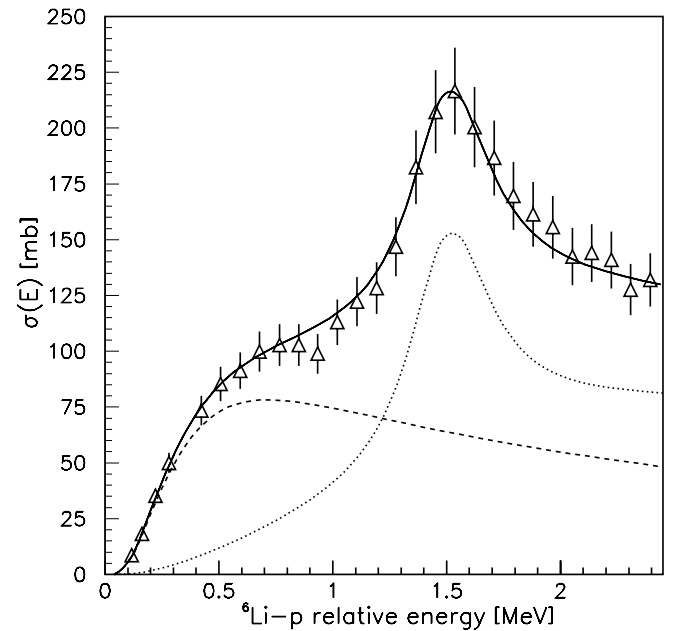


FIG. 6. Experimental cross section for the  ${}^6\text{Li}(p, \alpha){}^3\text{He}$  reaction from Ref. [22] (open triangles); full line, *R*-matrix fit to the experimental cross section for the same reaction; dashed and dotted lines, separate  $l=0$  and  $l=1$  contributions.

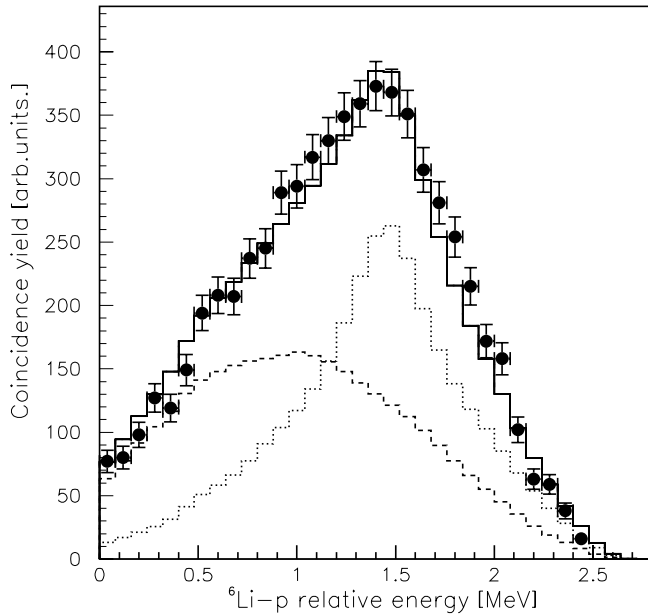


FIG. 7. Three-body coincidence yield projected on the  $p-{}^6\text{Li}$  relative energy (full circles); full line, calculated three-body cross section; dashed and dotted lines,  $l=0$  and  $l=1$  contributions.

with the separate  $l=0$  (dashed line) and  $l=1$  (dotted line) contributions. The calculation reproduces quite well the experimental behavior confirming the assumptions employed. The further step was to extract the two-body cross section from the coincidence yield in order to be compared with the two-body cross section from direct measurements. The appropriately scaled  $l=1$  contribution from the simulation of Fig. 7 was subtracted from the coincidence yield resulting in a smooth spectrum for the nonresonant  $s$ -wave contribution. This spectrum was first divided by the result of a Monte Carlo simulation for the  $l=0$  contribution, assuming a constant on-shell two-body cross section [see Eq. (10)], and then summed up to the  $l=1$  contribution from the  $R$ -matrix fit to the direct data (see Fig. 6). The result represents the two-body cross section extracted from the three-body reaction. Penetrability effects, due to the presence of both Coulomb (1.2 MeV) and centrifugal (3.9 MeV) barriers in the direct data, were fully accounted for in the procedure. The obtained two-body cross section is shown in Fig. 8 (full circles) and compared with the directly measured cross section (open triangles). The overall agreement is quite good with a distinct contribution from the resonance. The two sets of data are normalized to the top of the resonance and the reported experimental errors contain both statistical and normalization uncertainties, for an overall relative error of 11%. The  $\chi^2$  value of the fit to the direct data is 14.2 for 28 data points and one variable parameter, which accounts for the normalization between the two sets of data. A good agreement is a necessary condition for the applicability of the THM in the further extraction of the astrophysical  $S(E)$  factor and the  $\chi^2$  value can be considered as an important index of confidence for the performed validity test. Earlier works have already shown the consistency of the THM at energies above the two-body Coulomb barrier [15]. Furthermore, the method

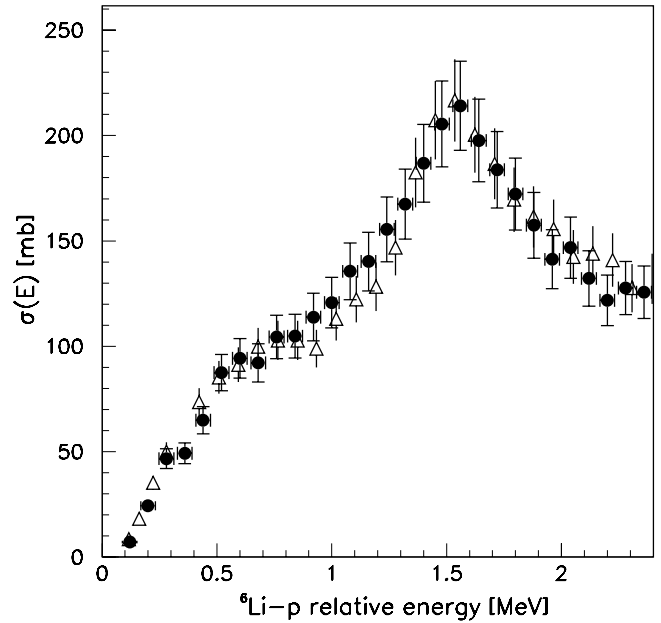


FIG. 8. Indirect  $p-{}^6\text{Li}$  two-body cross section (full circles) compared with the direct data from Ref. [22] (open triangles).

was checked also at sub-Coulomb energies [14,18]. The present result represents the first validity test spanning at the same time both energetic regions. The  $S(E)$  factor from the indirect data was then extracted and compared with the direct behavior, as shown in Fig. 9. For completeness, beside the data of Ref. [22] (open triangles), lower energy data of Ref. [25] (open circles) are reported and superimposed to ours (full circles). The full line represents the result of a second order polynomial fit to our data,  $S(E)=3.00-3.02E+1.93E^2$ , which gives a  $S(0)$  value of  $3.00 \pm 0.19$  MeV b. However, being the very low energy part of the  $S(E)$  spectrum in the tail of the detection efficiency curve, its behavior has to be further substantiated. An experimental study of the

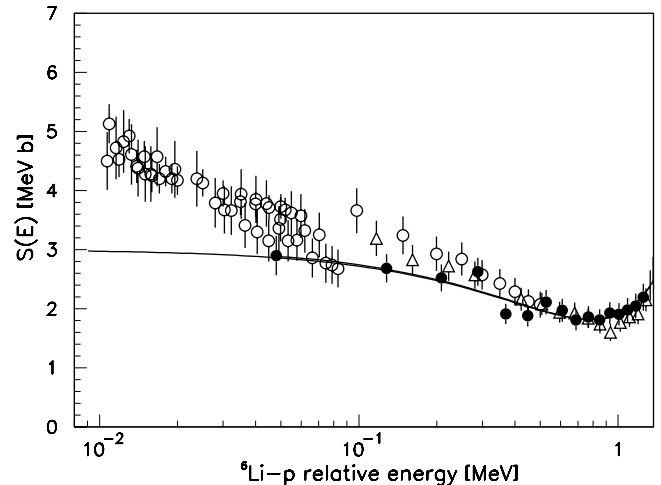


FIG. 9. Indirect  $p-{}^6\text{Li}$   $S(E)$  factor (full circles) compared with the direct data from Refs. [22] (open triangles) and [25] (open circles). The full line represents the result of a second order polynomial fit to the indirect data, as reported in the text.

$^2\text{H}(^6\text{Li}, \alpha^3\text{He})n$  reaction at lower beam energy will be performed in the near future, aimed at populating the energy region of astrophysical interest. A clear understanding of the low energy data, will help in defining the “transition” region where the disagreement between the two sets of data should be attributed to the presence of electron screening effects in the direct ones. This will allow us to get an estimate of the electron screening potential from the comparison of the two experimental trends.

## V. CONCLUSIONS

The obtained result on the  $^2\text{H}(^6\text{Li}, \alpha^3\text{He})n$  reaction establishes the presence of the quasifree mechanism around the

region of spectator momentum close to zero. The mechanism proceeds through a virtual two-body reaction of the incident  $^6\text{Li}$  with the proton in  $^2\text{H}$ . The  $p + ^6\text{Li}$  reaction was indirectly studied over a wide range of relative energy from 2.4 MeV down to the astrophysical region. The present work is of remarkable importance, being the first unified validity test for the THM below and above the Coulomb barrier. In a next step the same two-body reaction using  $^3\text{He}$  as Trojan horse nucleus instead of  $^2\text{H}$  will be studied. A relevant difference is the presence of a charged particle as spectator (the deuteron). This would allow to further test the dependence of the THM on the Trojan horse nucleus and on the spectator.

- 
- [1] G. Baur and H. Rebel, *J. Phys. G* **20**, 1 (1994), and references therein.
  - [2] G. Baur and H. Rebel, *Annu. Rev. Nucl. Part. Sci.* **46**, 321 (1996).
  - [3] J.G. Ross, G. Görres, C. Iliadis, S. Vouzoukas, M. Wiescher, R.B. Vogelaar, S. Utku, N.P.T. Batteman, and P.D. Parker, *Phys. Rev. C* **52**, 1681 (1995).
  - [4] C.A. Gagliardi, R.E. Tribble, A. Azhari, H.L. Clark, Y.W. Lui, A.M. Mukhamedzhanov, A. Sattarov, L. Trache, V. Burjan, J. Cejpek, V. Kroha, S. Piskor, and J. Vincour, *Phys. Rev. C* **59**, 1149 (1999).
  - [5] A. Azhari, V. Burjan, F. Carstoiu, H. Dejbakhsh, C.A. Gagliardi, V. Kroha, A.M. Mukhamedzhanov, L. Trache, and R.E. Tribble, *Phys. Rev. Lett.* **82**, 3960 (1999).
  - [6] C.A. Gagliardi, A. Azhari, V. Burjan, F. Carstoiu, V. Kroha, A.M. Mukhamedzhanov, A. Sattarov, X. Tang, L. Trache, and R.E. Tribble, *Eur. Phys. J. A* **13**, 227 (2002).
  - [7] G. Baur, *Phys. Lett. B* **178**, 135 (1986).
  - [8] S. Typel and H. Wolter, *Few-Body Syst.* **29**, 7 (2000).
  - [9] S. Typel and G. Baur, *Ann. Phys. (N. Y.)* (to be published), nucl-th/0208069.
  - [10] C.J. Copi, D.N. Schramm, and M.S. Turner, *Science* **627**, 192 (1995).
  - [11] L. Piau and S. Turck-Chieze, *Astrophys. J.* **566**, 419 (2002).
  - [12] M. Zadro, Dj. Miljanic, C. Spitaleri, G. Calvi, M. Lattuada, and F. Riggi, *Phys. Rev. C* **40**, 181 (1989).
  - [13] G. Calvi, S. Cherubini, M. Lattuada, S. Romano, C. Spitaleri, M. Aliotta, G. Rizzari, M. Sciuto, R.A. Zappalà, V.N. Kondratyev, Dj. Miljanic, M. Zadro, G. Baur, O.Yu. Goryunov, and A.A. Shvedov, *Nucl. Phys. A* **621**, 139c (1997).
  - [14] C. Spitaleri, M. Aliotta, S. Cherubini, M. Lattuada, Dj. Miljanic, S. Romano, N. Soić, M. Zadro, and R.A. Zappalà, *Phys. Rev. C* **60**, 055802 (1999).
  - [15] C. Spitaleri, M. Aliotta, P. Figuera, M. Lattuada, R.G. Pizzone, S. Romano, A. Tumino, C. Rolfs, L. Gialanella, F. Strieder, S. Cherubini, A. Musumarra, Dj. Miljanic, S. Typel, and H.H. Wolter, *Eur. Phys. J. A* **7**, 181 (2000).
  - [16] M. Lattuada, R.G. Pizzone, S. Typel, P. Figuera, Dj. Miljanic, A. Musumarra, M.G. Pellegriti, C. Rolfs, C. Spitaleri, and H.H. Wolter, *Astrophys. J.* **562**, 1076 (2001).
  - [17] S. Cherubini, V.N. Kondratyev, M. Lattuada, C. Spitaleri, Dj. Miljanic, M. Zadro, and G. Baur, *Astrophys. J.* **457**, 855 (1996).
  - [18] C. Spitaleri, S. Typel, R.G. Pizzone, M. Aliotta, S. Blagus, M. Bogovac, S. Cherubini, P. Figuera, M. Lattuada, M. Milin, Dj. Miljanic, A. Musumarra, M.G. Pellegriti, D. Rendić, C. Rolfs, S. Romano, N. Soić, A. Tumino, H.H. Wolter, and M. Zadro, *Phys. Rev. C* **63**, 055801 (2001).
  - [19] J.B. Marion, G. Weber, and F.S. Mozer, *Phys. Rev.* **104**, 1402 (1956).
  - [20] C.S. Lin, W.S. Hou, M. Wen, and J.C. Chou, *Nucl. Phys.* **A275**, 93 (1977).
  - [21] T. Shinozuka, Y. Tanaka, and K. Sugiyama, *Nucl. Phys.* **A326**, 47 (1979).
  - [22] A.J. Elwyn, R.E. Holland, C.N. Davids, L. Meyer-Schützmeister, F.P. Mooring, and W. Ray, Jr., *Phys. Rev. C* **20**, 1984 (1979).
  - [23] G. Calvi, M. Lattuada, Dj. Miljanic, F. Riggi, C. Spitaleri, and M. Zadro, *Phys. Rev. C* **41**, 1848 (1990).
  - [24] M. Jain *et al.*, *Nucl. Phys.* **A153**, 49 (1970).
  - [25] S. Engstler, G. Raimann, C. Angulo, U. Greife, C. Rolfs, U. Schröder, E. Somorjai, B. Kirch, and K. Langanke, *Z. Phys. A* **342**, 471 (1992).
  - [26] J.M.F. Jeronymo, G.S. Mani, and A. Sadeghi, *Nucl. Phys.* **43**, 424 (1963).
  - [27] U. Fasoli, D. Toniolo, and G. Zago, *Phys. Lett.* **8**, 127 (1964).
  - [28] W. Gemeinhardt, D. Kamke, and C. von Rheneck, *Z. Phys.* **197**, 58 (1966).
  - [29] H. Spinka, T. Tombrello, and H. Winkler, *Nucl. Phys.* **A164**, 1 (1971).
  - [30] C.R. Gould, R.O. Nelson, J.R. Williams, and J.R. Boyce, *Nucl. Sci. Eng.* **55**, 267 (1974).
  - [31] J.U. Kwon, J.C. Kim, and B.N. Sung, *Nucl. Phys.* **A493**, 112 (1989).
  - [32] C. Angulo *et al.*, *Nucl. Phys.* **A656**, 3 (1999).
  - [33] F.C. Barker, *Nucl. Phys.* **A707**, 277 (2002).